IEEE Access
Multidisciplinary | Rapid Review | Open Access Journal

Received September 14, 2020, accepted November 11, 2020, date of publication November 19, 2020,
date of current version December 7, 2020.

Digital Object Identifier 10.1109/ACCESS.2020.3039347

Multidimensional Information Fusion in Active Sonar via the Generalized Labeled Multi-Bernoulli Filter

XU SUN, RANWEI LI, AND LISHENG ZHOU
Hangzhou Applied Acoustics Research Institute, Hangzhou 310023, China

Corresponding author: Xu Sun (1513638732@qq.com)

This work was supported in part by the Navy Advance Research Program of China under Grant 3020202020102 and Grant 3020201030101.

ABSTRACT Under the conditions of low detection probabilities, high clutter rates, low data-sampling rates, large measurement errors, and unknown prior information of the target position, multi-object tracking is difficult. This paper proposes a multidimensional information fusion method in active sonar via the generalized labeled multi-Bernoulli (GLMB) filter. After modeling the position measurement, radial velocity measurement and amplitude measurement of the target and clutter, new target births are adaptively generated by the measurement-driven model, predictions are made by the target motion model and updates are performed via multidimensional measurements with the generalized likelihood in the GLMB filter, which enables the measurement information of different dimensions to be elegantly applied to information fusion and significantly improves the filter performance. The contribution of specific dimension measurement to fusion can be evaluated by the Kullback-Leibler (KL) divergence. In the efficient implementation, we propose flat Gibbs sampling to realize multiple hypothesis optimization. Moreover, the filtering recursion is derived from Gaussian mixtures. Simulations are presented to verify the proposed method.

INDEX TERMS Random finite sets, generalized labeled multi-Bernoulli filter, multidimensional information fusion, flat Gibbs sampling.

I. INTRODUCTION

In the complex and changeable marine environment, the acoustic scattering caused by an uneven seabed [1], [2], rolling surfaces [3], fish in the water, and the noise of human activities, such as navigation, fishing, and underwater mining, lead to substantial clutter interference in submarine detection using active sonar. The energy of an acoustic signal rapidly attenuates when the signal propagates under water [4], and the weak echo signal often causes target missed detection. In addition, active sonar works at a low frequency and over a limited bandwidth with a small array aperture, which results in a large measurement error. Moreover, the acoustic velocity in water is relatively slow, and the detection time covering a certain range is long, which results in a low detection data rate. Thus, the multi-object tracking in active sonar faces four challenges: low detection probabilities, high clutter rates, low data rates and large measurement errors.

The associate editor coordinating the review of this manuscript and approving it for publication was Taous Meriem Laleg-Kirati.

The objective of multi-object tracking is to jointly estimate the number of targets and their trajectories from a sequence of noisy and cluttered observation sets in the presence of unknown prior information of new target births. Three major algorithms have been developed: joint probability data association filtering (JPDA) [5], multiple hypothesis tracking (MHT) [6], [7], and random finite set (RFS) [8]–[10]. RFS is rigorous, elegant, and suitable for the multidimensional heterogeneous information fusion and semantic target information fusion scenarios to which traditional methods are difficult to apply. Led by Mahler and Vo-Vo, a group of outstanding scholars engaged in this work and successively proposed the implementation methods of probability hypothesis density (PHD) filter [11] and its cardinalized version, cardinalized PHD (CPHD) [12], the multi-target multi-Bernoulli (MeMBer) filter [8], [13], and the newly derived generalized labeled multi-Bernoulli (GLMB) filter [14]–[16] and its special case, the labeled multi-Bernoulli (LMB) filter [17]–[19]. Among them, GLMB filtering is based on the labeled RFS theory and strictly derived, which has better cardinality

estimation accuracy and OSPA metric [20], [21] performances than PHD, CPHD, and MeMBer. Therefore, we study the multidimensional information fusion and multi-object tracking in active sonar based on GLMB.

Under the conditions of low detection probabilities, high clutter rates, low data-sampling rates, and large measurement errors in active sonar, the performance of the GLMB filter is seriously degraded. In [22], [23], the A-PHD filter was proposed based on the echo amplitude information, through which the variance in the cardinality estimation was significantly reduced compared to the PHD filter. In [24], [25], the echo amplitude information was also used to propose the A-LMB filter, which was applied to radar target tracking and achieved better processing results than the LMB filter. Using the multidimensional measurement information, we propose a multidimensional information fusion method via the generalized labeled multi-Bernoulli (MDI-GLMB) filter. Our main innovations are as follows:

- Multidimensional measurement modeling.

In the GLMB update step, the position measurement, radial velocity measurement and amplitude measurement of the target and clutter are modeled, and the generalized likelihood of the measurement is calculated. Multidimensional information fusion is implemented in the active sonar.

- Evaluation of the contribution of certain information to fusion by the Kullback-Leibler divergence [26].

In multidimensional measurement, each measurement dimension has a different ability to distinguish the target and clutter, and its contribution to information fusion also differs. Thus, the contribution evaluation based on the relative entropy (Kullback-Leibler divergence, or simply the KL divergence) is proposed.

- Flat Gibbs sampling.

In the MDI-GLMB filter, in addition to position measurement, amplitude measurement and radial velocity measurement are also included. The finite Gibbs sampling [15], [27]–[29] method fails to achieve multiple hypothesis optimization. A flat Gibbs sampling method is proposed to achieve robust multiple hypothesis optimization.

The paper is organized as follows. Background on active sonar target measurement, the GLMB filter, and the unscented Kalman filter (UKF) is provided in Section II. In Section III, the position measurement, radial velocity measurement and amplitude measurement of the target and clutter are modeled. Section IV presents the implementation of the MDI-GLMB filter. Numerical results are presented in Section V, and concluding remarks are given in Section VI.

II. BACKGROUND

This section briefly introduces the background of active sonar measurement, the UKF, and GLMB filtering. Readers can refer to [4], [15], [30] for detailed expositions. For the convenience of subsequent description, we first present the following notations and definitions. Single-object states are represented by lowercase letters (e.g., x, $\mathbf{x}$), while multi-object states are represented by uppercase letters (e.g., X, $\mathbf{X}$). Symbols for labeled states and their distributions are bolded (e.g., $\mathbf{x}$, $\mathbf{X}$, $\boldsymbol{\pi}$) to distinguish them from unlabeled states, and spaces are represented by blackboard bold (e.g., $\mathbb{X}$, $\mathbb{Z}$, $\mathbb{L}$).

A. ACTIVE SONAR MEASUREMENT

Active sonar usually uses the combined hyperbolic frequency modulation and single frequency signals to detect targets, which can be used to simultaneously measure the target position, echo amplitude and target radial velocity. The measurement of target i at time k can be expressed as

$$z_k^{(i)} = \left[\theta_k^{(i)},\ r_k^{(i)},\ \dot{r}_k^{(i)},\ a_k^{(i)}\right].$$

Note that SL represents the source level of active sonar, TL represents the acoustic transmission loss, NL represents the noise level of the marine environment, TS represents the target strength, GT and GS represent the time processing gain and spatial processing gain, respectively, and SNR represents the echo signal-to-noise ratio. The active sonar equation is

$$SNR = SL - 2TL - NL + TS + GT + GS \tag{1}$$

In [22], [24], [25], the Rayleigh distribution describes the amplitude fluctuation of the target and clutter. The probability density functions of the clutter and target amplitudes are expressed as follows:

$$g(a) = a\exp\left(\frac{-a^2}{2}\right), \quad a \geq 0 \tag{2}$$

$$g(a\,|d) = \frac{a}{1+d}\exp\left(\frac{-a^2}{2\,(1+d)}\right), \quad a \geq 0. \tag{3}$$

The expected SNR is $1+d$, which is typically defined in the log scale as $SNR\,(\mathrm{dB}) = 10\log_{10}(1+d)$.

The SNR of the target echo can be estimated from the active sonar equation, and the detection probability (P_D) of the target can be calculated based on the detection threshold and probability distribution. $z_k^{(i)}$ may or may not be detected,

$$\emptyset, \quad \left[\theta_k^{(i)},\ r_k^{(i)},\ \dot{r}_k^{(i)},\ a_k^{(i)}\right].$$

where $\emptyset$ indicates that $z_k^{(i)}$ is missed.

B. UKF IN MDI-GLMB

The observation model of active sonar is nonlinear, in which the UKF is applied to the continuous measurement of the target position and radial velocity for state estimation. The target state equation is

$$x_{k+1}^{(i)} = F_k x_k^{(i)} + \Gamma_k u_k \tag{4}$$

where $x_k^{(i)}$ is the state vector of target i at time k, F_k is the state transition matrix, Γ_k is the process noise distribution matrix, and u_k is the process noise vector. Assuming Δ as the period,

$$x_k^{(i)} = \left[p_{x,k}^{(i)},\ \dot{p}_{x,k}^{(i)},\ p_{y,k}^{(i)},\ \dot{p}_{y,k}^{(i)}\right]^T, \quad u_k = [u_x,\ u_y]^T,$$

$$F_k = \begin{bmatrix} 1 & \Delta & 0 & 0 \\ 0 & 1 & 0 & 0 \\ 0 & 0 & 1 & \Delta \\ 0 & 0 & 0 & 1 \end{bmatrix}, \quad \Gamma_k = \begin{bmatrix} 0.5\Delta^2 & 0 \\ \Delta & 0 \\ 0 & 0.5\Delta^2 \\ 0 & \Delta \end{bmatrix}.$$

The measurement equation can be expressed as (5), as shown at the bottom of the next page where $w_k^{(i)}$ is the measurement noise, $w_k^{(i)} \sim N\left(0, R_k^i\right)$; R_k^j is the covariance of the measurement noise, in which $R_k^i = diag\left(\left[\sigma_\theta^2, \sigma_r^2, \sigma_v^2\right]\right)$.

Using the unscented transform (UT) for the nonlinear observation model in the UKF, the predicted measurement is

$$z_{k+1|k}^{(i)} = \sum_{n=1}^{2n_x+1} w^n h\left(\xi_{k+1}^{(i,n)}\right) \quad n = 1, 2, \cdots, 2n_x + 1 \tag{6}$$

where n_x is the dimension of the state vector, $n_x = 4$; $\xi_{k+1}^{(i,n)}$ represents a state sample of target i with weight w^n.

The UKF recursion equations based on the filter model of active sonar are provided for convenience as follows:

$$x_{k+1|k}^{(i)} = F_k x_k^{(i)} \tag{7}$$

$$P_{k+1|k}^{(i)} = F_k P_k^{(i)} F_k^{\mathrm{T}} + Q_k \tag{8}$$

$$S_{k+1}^{(i)} = R_{k+1}^{(i)} + \sum_{n=1}^{2n_x+1} w^n \left[h\left(\xi_{k+1}^{(i,n)}\right) - z_{k+1|k}^{(i)}\right] \times \left[h\left(\xi_{k+1}^{(i,n)}\right) - z_{k+1|k}^{(i)}\right]^T \tag{9}$$

$$K_{k+1}^{(i)} = \sum_{n=1}^{2n_x+1} w^n \left[\xi_{k+1}^{(i,n)} - x_{k+1|k}^{(i)}\right] \times \left[h\left(\xi_{k+1}^{(i,n)}\right) - z_{k+1|k}^{(i)}\right]^{\mathrm{T}} \left(S_{k+1}^{(i)}\right)^{-1} \tag{10}$$

$$v_{k+1}^{(i)} = z_{k+1}^{(i)} - z_{k+1|k}^{(i)} \tag{11}$$

$$x_{k+1}^{(i)} = x_{k+1|k}^{(i)} + K_{k+1}^{(i)} v_{k+1}^{(i)} \tag{12}$$

$$P_{k+1}^{(i)} = P_{k+1|k}^{(i)} - K_{k+1}^{(i)} S_{k+1}^{(i)} \left(K_{k+1}^{(i)}\right)^{\mathrm{T}} \tag{13}$$

where $x_{k+1|k}^{(i)}$ is the state prediction vector, $P_k^{(i)}$ is the state error covariance matrix, $P_{k+1|k}^{(i)}$ is the error covariance matrix of the prediction state, $S_{k+1}^{(i)}$ is the innovation covariance matrix, $v_{k+1}^{(i)}$ denotes the innovation, $K_{k+1}^{(i)}$ is the filter gain, and Q_k is the process noise covariance matrix.

When measurement of the target is missed, the update step is

$$x_{k+1}^{(i)} = x_{k+1|k}^{(i)} \tag{14}$$

$$P_{k+1}^{(i)} = P_{k+1|k}^{(i)} \tag{15}$$

C. LABELED RFS AND GLMB FILTER

Denote a generalization of the Kronecker delta, which takes arbitrary arguments such as sets, vectors, and integers, as follows:

$$\delta_Y[X] \triangleq \begin{cases} 1, & \text{if } X = Y \\ 0, & \text{otherwise.} \end{cases}$$

For a given set S, $1_S(\cdot)$ denotes the indicator function of S, and $\mathcal{F}(S)$ denotes the class of finite subsets of S. For a finite set X, its cardinality (number of elements) is denoted by $|X|$. In addition, we denote by f^X the multi-object exponential, where $f^X = \prod_{x \in X} f(x)$ and $f^{\emptyset} = 1$; $\langle f, g \rangle$ denotes the inner product, $\langle f, g \rangle = \int f(x) g(x) dx$.

To estimate the identity or trajectory of a target in a multi-object scenario, a state $x \in \mathbb{X}$ is augmented by a label $l \in \mathbb{L}$, that is, $\mathbf{x} = (x, l)$. Labels for individual targets are ordered as pairs of integers $l = (k, i)$, where k is the birth time of the new target, and i is a unique index to distinguish new targets born at the same time. The label set of a labeled RFS $\mathbf{X}$ is given by $\mathcal{L}(\mathbf{X}) = \{\mathcal{L}(\mathbf{x}) : \mathbf{x} \in \mathbf{X}\}$, where $\mathcal{L} : \mathbb{X} \times \mathbb{L} \to \mathbb{L}$ is the projection defined by $\mathcal{L}((x, l)) = l$. The labels of targets in $\mathbf{X}$ must be distinct, i.e., $|\mathcal{L}(\mathbf{X})| = |\mathbf{X}|$.

In the implementation of the GLMB filter, known as $\delta - GLMB$, its filtering density at time k is

$$\boldsymbol{\pi}(\mathbf{X}) = \Delta(\mathbf{X}) \sum_{\xi \in \Xi, I \in \mathcal{F}(\mathbb{L})} w^{(I,\xi)} \delta_I[\mathcal{L}(\mathbf{X})] \left[p^{(\xi)}\right]^{\mathbf{X}} \tag{16}$$

where $\Delta(\mathbf{X})$ is the distinct label indicator, $\Delta(\mathbf{X}) = \delta_{|\mathbf{X}|}[\mathcal{L}(\mathbf{X})]$, and $w^{(I,\xi)} = w^{(\xi)}(I)$. Each $\xi \in \Xi$ represents a history of association maps $\xi = (\theta_{1:k})$, while each $I \in \mathcal{F}(\mathbb{L})$ represents a set of object labels. Each pair (I, ξ) with weight $w^{(I,\xi)}$ and distribution $p^{(\xi)}$ represents a possible association between targets and measurements, and clearly, $\sum_{\xi \in \Xi, I \in \mathcal{F}(\mathbb{L})} w^{(I,\xi)} = 1$.

The predicted density of $\delta - GLMB$ is

$$\bar{\boldsymbol{\pi}}_+(\mathbf{X}) = \Delta(\mathbf{X}) \sum_{\xi, J, L_+} \bar{w}_+^{(\xi,J,L_+)} \delta_{J \cup L_+}[\mathcal{L}(\mathbf{X})] \left[\bar{p}_+^{(\xi)}\right]^{\mathbf{X}} \tag{17}$$

where $\xi \in \Xi$, $J \in \mathcal{F}(\mathbb{L})$, $L_+ \in \mathcal{F}(\mathbb{B})$, and

$$\bar{w}_+^{(\xi,J,L_+)} = 1_{\mathcal{F}(\mathbb{B})}(L_+) r_{B,+}^{L_+} \left[1 - r_{B,+}\right]^{\mathbb{B}_+ - L_+} \times \sum_{I \in \mathcal{F}(\mathbb{L})} 1_{\mathcal{F}(I)}(J) \left[\bar{P}_S^{(\xi)}\right]^J \left[1 - \bar{P}_S^{(\xi)}\right]^{I-J} \tag{18}$$

$$\bar{P}_S^{(\xi)} = \left\langle p^{(\xi)}(\cdot, l), P_S(\cdot, l) \right\rangle \tag{19}$$

$$\bar{p}_+^{(\xi)}(x_+, l_+) = 1_{\mathbb{L}}(l_+) \frac{\left\langle P_S(\cdot, l_+) f_+(x_+ | \cdot, l_+), p^{(\xi)}(\cdot, l_+) \right\rangle}{\bar{P}_S^{(\xi)}(l_+)} + 1_{\mathbb{B}_+}(l_+) p_{B,+}(x_+, l_+) \tag{20}$$

where $r_{B,+}^{l_+}$ is the probability of a newborn target with label l_+, and $p_{B,+}(x_+, l_+)$ is the distribution of its kinematic state. $P_S(\cdot, l)$ is the probability if target l exists. $f_+(x_+ | \cdot, l_+)$ is the probability density from state (x, l) to new state (x_+, l_+).

Then, the updated density in $\delta - GLMB$ filtering at time $k+1$ is

$$\boldsymbol{\pi}_{Z_+}(\mathbf{X}) \propto \Delta(\mathbf{X}) \sum_{\xi, J, L_+, \theta_+} w_{Z_+}^{(\xi,J,L_+,\theta_+)} \delta_{J \cup L_+}[\mathcal{L}(\mathbf{X})] \times \left[p_{Z_+}^{(\xi,\theta_+)}\right]^{\mathbf{X}} \tag{21}$$

where $\theta_+ \in \Theta_+$, and

$$w_{Z_+}^{(\xi,J,L_+,\theta_+)} = 1_{\Theta_+(J\cup L_+)}(\theta_+)\left[\bar{\varphi}_{Z_+}^{(\xi,\theta_+)}\right]^{J\cup L_+} \bar{w}_+^{(\xi,J,L_+)} \tag{22}$$

$$\bar{\varphi}_{Z_+}^{(\xi,\theta_+)}(l_+) = \left\langle \bar{p}_+^{(\xi)}(\cdot,l_+), \varphi_{Z_+}^{(\theta_+(l_+))}(\cdot,l_+)\right\rangle \tag{23}$$

$$p_{Z_+}^{(\xi,\theta_+)}(x_+,l_+) = \frac{\bar{p}_+^{(\xi)}(x_+,l_+)\,\varphi_{Z_+}^{(\theta_+(l_+))}(x_+,l_+)}{\bar{\varphi}_{Z_+}^{(\xi,\theta_+)}(l_+)} \tag{24}$$

where Θ is the set of association maps θ. The map θ specifies which targets generated which measurements, i.e., target l generates measurement $z_{\theta(l)} \in Z$. When target l is undetected, $\theta(l) = 0$. The multi-object likelihood function is

$$g(Z|\mathbf{X}) \propto \sum_{\theta\in\Theta} 1_{\Theta(\mathcal{L}(\mathbf{X}))}(\theta) \prod_{(x,l)\in\mathbf{X}} \varphi_Z^{(\theta(l))}(x,l) \tag{25}$$

In association maps θ, a measurement is associated with at most one target, and a target is also associated with at most one measurement. For a possible domain I, $\Theta(I) \subseteq \Theta$, the likelihood of target $l \in I$ with measurement j is

$$\varphi_{\{z_{1:|Z|}\}}^{(j)}(x,l) = \begin{cases} \dfrac{P_D(x,l)\, g\left(z_j|x,l\right)}{k\left(z_j\right)}, & \text{if } j\in\{1,\cdots,|Z|\} \\ 1-P_D(x,l), & \text{if } j=0 \end{cases} \tag{26}$$

where $g\left(z_j|x,l\right)$ is the target measurement likelihood, and $k\left(z_j\right)$ is the intensity of the Poisson clutter.

III. MULTIDIMENSIONAL MEASUREMENT MODELING

GLMB filtering was implemented in [14], [15] using only position measurements of the target and clutter. In [24], [25], amplitude information aided LMB filtering (i.e., A-LMB) was proposed. We further model multidimensional measurements (position, radial velocity and echo amplitude) in active sonar, calculating the target likelihood and clutter likelihood, which can be used in the update step of the GLMB filter.

A. POSITION MEASUREMENT

Normally, the location of clutter is unknown. Assuming that it is uniformly distributed in the two-dimensional plane of azimuth and range, the intensity function of clutter modeled by a Poisson RFS is

$$k\left(z_j^{(\theta,\gamma)}\right) = \lambda_c \tag{27}$$

where λ_c is the intensity of clutter.

In continuous multiple scans in active sonar, the position measurements of the same target are adjacent, and we can predict the target position based on the target motion model. The likelihood function of $z_j^{(\theta,\gamma)}$ from target l_i is

$$\begin{aligned} &g\left(z_j^{(\theta,r)}\middle| x_i,l_i\right) \\ &= \frac{1}{2\pi\cdot\left(\det S_p^{(i)}\right)^{1/2}} \\ &\cdot\exp\left[-\frac{1}{2}\left(z_j^{(\theta,r)}-z_{p,i}^{(\theta,r)}\right)^T\left(S_p^{(i)}\right)^{-1}\left(z_j^{(\theta,r)}-z_{p,i}^{(\theta,r)}\right)\right] \end{aligned} \tag{28}$$

where $S_p^{(i)}$ is the position innovation covariance matrix of target l_i. $\det(\cdot)$ represents the matrix determinant operation. $z_{p,i}^{(\theta,r)}$ is the predicted position measurement of target l_i.

To intuitively show the difference in the likelihood probability density function between the target and clutter in position measurement intuitively, assume that $S_p^{(i)} = \mathrm{diag}\left(\left[\pi/180, 100\right]^2\right)$ and $\lambda_c = 1$. The position measurement likelihood probability density functions of the target (shown in pseudocolor) and clutter (shown in the blue-green plane) can be drawn as in Fig. 1.

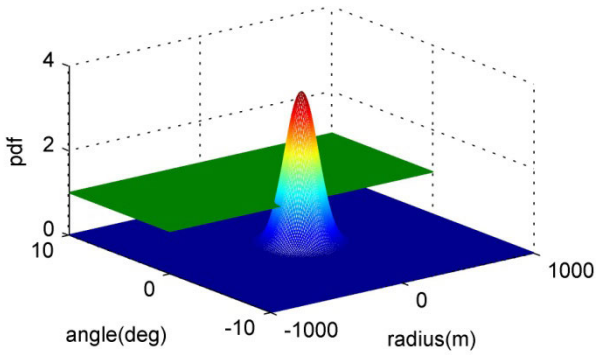

FIGURE 1. Position measurement likelihood probability density functions of the target and clutter.

B. RADIAL VELOCITY MEASUREMENT

Clutter is mainly formed by the sound scattering from the seabed and surface in active sonar. Therefore, the radial velocity measurement of clutter obeys a zero mean Gaussian distribution. The likelihood function of $z_j^{(\dot{r})}$ from clutter is

$$g_{\dot{r}}\left(z_j^{(\dot{r})}\middle| c\right) = \frac{1}{\sqrt{2\pi S_{\dot{r}}^{(i)}}}\exp\left(-\frac{\left(z_j^{(\dot{r})}\right)^2}{2S_{\dot{r}}^{(i)}}\right) \tag{29}$$

In the UKF, position measurement and radial velocity measurement are used for filtering processing, and the likelihood

$$z_k^{(i)} = h\left(x_k^{(i)}\right) + w_k^{(i)} = \left[\arctan\left(p_{y,k}^{(i)}/p_{x,k}^{(i)}\right), \sqrt{\left(p_{x,k}^{(i)}\right)^2+\left(p_{y,k}^{(i)}\right)^2}, \frac{p_{x,k}^{(i)}\dot{p}_{x,k}^{(i)}+p_{y,k}^{(i)}\dot{p}_{y,k}^{(i)}}{\sqrt{\left(p_{x,k}^{(i)}\right)^2+\left(p_{y,k}^{(i)}\right)^2}}\right]^T + w_k^{(i)} \tag{5}$$

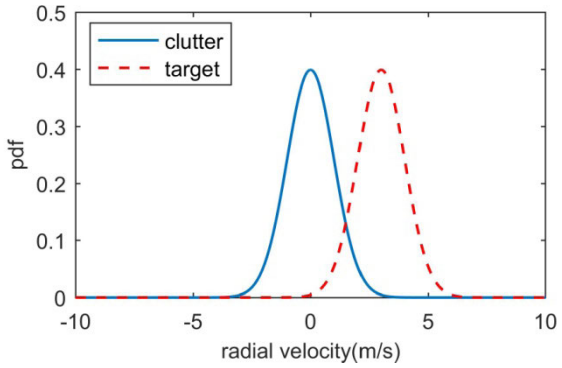

FIGURE 2. Radial velocity measurement likelihood probability density functions of the target and clutter.

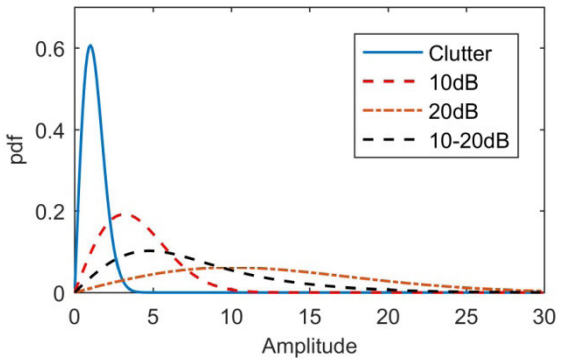

FIGURE 3. Amplitude measurement likelihood probability density functions of targets and clutter.

function of $z_j^{(\dot{r})}$ from target l_i is

$$g_{\dot{r}}\left(z_j^{(\dot{r})}\middle| x_i, l_i\right) = \frac{1}{\sqrt{2\pi S_{\dot{r}}^{(i)}}} \exp\left(-\frac{\left(z_j^{(\dot{r})} - z_{p,i}^{(\dot{r})}\right)^2}{2S_{\dot{r}}^{(i)}}\right) \tag{30}$$

where $z_{p,i}^{(\dot{r})}$ is the radial velocity prediction of target l_i, and $S_{\dot{r}}^{(i)}$ represents the radial velocity innovation covariance of target l_i.

To intuitively show the difference in the likelihood probability density function between the target and clutter in radial velocity measurement, assume that $S_{\dot{r}}^{(i)} = 1$ and $z_{p,i}^{(\dot{r})} = 3m/s$. The radial velocity measurement likelihood probability density functions of the target (shown as the red-dotted line) and clutter (shown as the blue-solid line) can be drawn as in Fig. 2.

C. AMPLITUDE MEASUREMENT

The amplitude measurement likelihood probability density functions of the target and clutter are given in the background section, specifically shown in (2) and (3). However, measurement sets are obtained based on CFAR detection. Note that τ represents the detection threshold and P_{fa}^{τ} represents the false alarm probability. The amplitude measurement of the target and clutter must be greater than or equal to the detection threshold, that is, $z_j^{(a)} \geq \tau$. The likelihood function of $z_j^{(a)}$ from clutter is

$$g_a^{\tau}\left(z_j^{(a)}\middle| c\right) = \frac{1}{P_{fa}^{\tau}} z_j^{(a)} \exp\left(\frac{-\left(z_j^{(a)}\right)^2}{2}\right), \quad z_j^{(a)} \geq \tau \tag{31}$$

Suppose that the SNR of target l_i is $1 + d$. The likelihood function of $z_j^{(a)}$ from target l_i is

$$g_a^{\tau}\left(z_j^{(a)}\middle| d, l_i\right) = \frac{1}{P_D^{\tau}} \frac{z_j^{(a)}}{1+d} \exp\left(\frac{-\left(z_j^{(a)}\right)^2}{2(1+d)}\right), \quad z_j^{(a)} \geq \tau \tag{32}$$

where P_D^{τ} is the probability of detection; obviously, $g_a\left(z_j^{(a)}\middle| d, l_i\right) = P_D^{\tau} g_a^{\tau}\left(z_j^{(a)}\middle| d, l_i\right)$.

Generally, the underwater acoustic channel and target attitude are time-varying, which leads to estimation error of the target SNR based on the active sonar equation. To solve this problem, we use the method in [22], [23], where the modeled target SNR is uniformly distributed in [dB1, dB2]. The likelihood function of $z_j^{(a)}$ from target l_i is (33), as shown at the bottom of the next page where $\mathrm{dB1\,(dB)} = 10\log_{10}(1+d_1)$; $\mathrm{dB2\,(dB)} = 10\log_{10}(1+d_2)$; P_{2D}^{τ} is the probability of detection; Obviously, $g_a\left(z_j^{(a)}\middle| d_1, d_2, l_i\right) = P_{2D}^{\tau} g_a^{\tau}\left(z_j^{(a)}\middle| d_1, d_2, l_i\right)$.

To intuitively show the difference in the likelihood probability density function between the target and clutter in amplitude measurement, we have drawn Fig. 3. In this figure, 10 dB (shown as the red-dotted line), 20 dB (shown as the blue-dotted line) and 10-20 dB (shown as the black-dotted line) targets are selected for comparison with clutter (shown as the blue-solid line).

D. GENERALIZED LIKELIHOOD OF MULTIDIMENSIONAL MEASUREMENT

We denote the implementation of GLMB filtering that only uses position measurement [8], [9] as GLMB in this paper. The likelihood of the jth measurement associated with target l_i is

$$\psi_Z^{(j)}(x_i, l_i) = \begin{cases} P_D^{\tau}(x_i, l_i)\, g\left(z_j^{(\theta,r)}\middle| x_i, l_i\right) \Big/ k\left(z_j^{(\theta,r)}\right), & j > 0 \\ 1 - P_D^{\tau}(x_i, l_i), & j = 0 \end{cases} \tag{34}$$

We denote the implementation of GLMB filtering that jointly uses position and radial velocity measurement as V-GLMB. The likelihood of the jth measurement associated with target l_i is

$$\psi_Z^{(j)}(x_i, l_i) = \begin{cases} \dfrac{P_D^{\tau}(x_i, l_i)\, g\left(z_j^{(\theta,r)}\middle| x_i, l_i\right) g_{\dot{r}}\left(z_j^{(\dot{r})}\middle| x_i, l_i\right)}{k\left(z_j^{(\theta,r)}\right) g_{\dot{r}}\left(z_j^{(\dot{r})}\middle| c\right)}, \\ \quad j > 0 \\ 1 - P_D^{\tau}(x_i, l_i), \\ \quad j = 0 \end{cases} \tag{35}$$

We denote the implementation of GLMB filtering that uses position and amplitude measurement in combination as A-GLMB. The likelihood of the jth measurement associated with target l_i is

$$\psi_Z^{(j)}(x_i, l_i) = \begin{cases} \dfrac{P_D^{\tau}(x_i, l_i)\, g\left(z_j^{(\theta,r)} \middle| x_i, l_i\right)\left(P_D^{\tau} g_a^{\tau}\left(z_j^{(a)} \middle| d, l_i\right)\right)}{k\left(z_j^{(\theta,r)}\right)\left(P_{fa}^{\tau} g_a^{\tau}\left(z_j^{(a)} \middle| n\right)\right)}, \\ \quad j > 0 \\ 1 - P_D^{\tau}(x_i, l_i), \\ \quad j = 0 \end{cases} \tag{36}$$

We denote the implementation of GLMB filtering with multidimensional (e.g., joint position, radial velocity and amplitude) measurement as MDI-GLMB. The likelihood of the jth measurement associated with target l_i is (37), as shown at the bottom of the next page.

E. ANALYSIS OF THE KL DIVERGENCE

In multidimensional measurement, each measurement dimension has a different ability to distinguish the target and clutter, and its contribution to information fusion also differs. The KL divergence is proposed in this paper to evaluate the contribution of each measurement dimension. The KL divergence [26] is a physical quantity to measure the difference degree of two probability distributions. A larger KL divergence corresponds to a greater difference between the two distributions; intuitively, a greater difference between target and clutter in the probability distributions corresponds to an easier clutter reduction or better performance in the OSPA metric and cardinality estimation.

The KL divergence of the target and clutter in position measurement is

$$D_{KL}^{(\theta,r)} = \iint P_D^{\tau}(x_i, l_i)\, g\left(z_j^{(\theta,r)} \middle| x_i, l_i\right) \times \log\left(\frac{P_D^{\tau}(x_i, l_i)\, g\left(z_j^{(\theta,r)} \middle| x_i, l_i\right)}{k\left(z_j^{(\theta,r)}\right)}\right) r dr d\theta \tag{38}$$

The KL divergence of the target and clutter in radial velocity measurement is

$$D_{KL}^{(\dot{r})} = \int g_{\dot{r}}\left(z_j^{(\dot{r})} \middle| x_i, l_i\right) \log\left(\frac{g_{\dot{r}}\left(z_j^{(\dot{r})} \middle| x_i, l_i\right)}{g_{\dot{r}}\left(z_j^{(\dot{r})} \middle| c\right)}\right) d\dot{r} \tag{39}$$

TABLE 1. KL divergence between the target and the clutter in different scenarios.

Scenario parameters: False alarm rate, 0.001; range,25 km; Radial velocity, $z_j^{(\dot{r})} = 2$.	$D_{KL}^{(\theta,r)}$	$D_{KL}^{(\dot{r})}$	$D_{KL}^{(a)}$
Weak target, SNR=10 dB; $\lambda_c = 3.82\times10^{-4} m^{-1}(rad)^{-1}$; innovation covariance, $S^{(i)} = \mathrm{diag}\left(\left[8\pi/180, 400, 1\right]^2\right)$.	35.48	2.00	6.70
General target, SNR=20 dB; $\lambda_c = 3.82\times10^{-4} m^{-1}(rad)^{-1}$; innovation covariance, $S^{(i)} = \mathrm{diag}\left(\left[4\pi/180, 200, 0.5\right]^2\right)$.	97.89	8.00	94.39

The KL divergence of the target and clutter in amplitude measurement is

$$D_{KL}^{(a)} = \int g_a\left(z_j^{(a)} \middle| d, l_i\right) \log\left(\frac{g_a\left(z_j^{(a)} \middle| d, l_i\right)}{g_a\left(z_j^{(a)} \middle| c\right)}\right) da \tag{40}$$

Table 1 shows the values of $D_{KL}^{(\theta,r)}$, $D_{KL}^{(\dot{r})}$ and $D_{KL}^{(a)}$ in two typical application scenarios. The KL divergence in each measurement dimension is greater than zero, which indicates that the measurement of each dimension contributes to information fusion. The implementation of the MDI-LMB filter will be able to achieve better performance in multi-object tracking in active sonar.

IV. IMPLEMENTATION OF MDI-GLMB

In this section, we will introduce the implementation of the MDI-GLMB filter in detail. First, new targets are generated based on the measurement-driven birth model under the condition that their initial position and intensity are unknown. Second, the joint prediction and update step is performed. Finally, a flat Gibbs sampling method is proposed to achieve multiple hypothesis optimization.

A. MEASUREMENT-DRIVEN BIRTH

The standard implementation of the RFS filter relies on a priori knowledge of newborn targets; however, this knowledge is unknown in active sonar. Based on the measurement-driven model [17], [33]–[35], we can adaptively generate new targets and their distribution. The measurement sets at time k (denoted Z_k) are used to generate new targets at time $k+1$. Therefore, the multi-Bernoulli birth distribution at time $k+1$ (denoted $\boldsymbol{\pi}_{B,k+1}$) is

$$\boldsymbol{\pi}_{B,k+1} = \left\{r_{B,k}^{(l)}(z), p_{B,k}^{(l)}(x|z) : l = l_B(z)\right\}_{z\in Z_k} \tag{41}$$

$$g_a^{\tau}\left(z_j^{(a)} \middle| d_1, d_2, l_i\right) = \frac{2}{P_{2D}^{\tau} z_j^{(a)}}\left[\exp\left(\frac{-\left(z_j^{(a)}\right)^2}{2(1+d_2)}\right) - \exp\left(\frac{-\left(z_j^{(a)}\right)^2}{2(1+d_1)}\right)\right] \Big/ \left[\ln(1+d_2) - \ln(1+d_1)\right], \quad z_j^{(a)} \geq \tau \tag{33}$$

where $l_B(z)$ is the label of a newborn target driven by measurement $z \in Z_k$; the birth probability and probability distribution of the newborn target are $r_{B,k}^{(l)}(z)$ and $p_{B,k}^{(l)}(x|z)$, respectively.

The probability density of the newborn GLMB is

$$\boldsymbol{\pi}_B(\mathbf{X}_+) = \Delta(\mathbf{X}_+) w_B(\mathcal{L}(\mathbf{X}))[p_B]^{\mathbf{X}} \tag{42}$$

where

$$w_B(I) = \prod_{i\in\mathbb{B}}\left(1 - r_B^{(i)}\right)\prod_{l\in I}\frac{1_{\mathbb{B}}(l) r_B^{(l)}}{1 - r_B^{(l)}} \tag{43}$$

The new-born likelihood for each measurement $z \in Z_k$ can be found by

$$r_{U,k}(z) = 1 - \sum_{(I,\xi)\in\mathcal{F}(\mathbb{L})\times\Xi}\sum_{\theta\in\Theta(I)} 1_{z_\theta}(z) w^{(I,\xi,\theta)} \tag{44}$$

where $w^{(I,\xi,\theta)}$ can be given by the GLMB filter from the last time. Clearly, a measurement that has been used in all hypotheses cannot generate a newborn target ($r_{U,k}(z) = 0$), while for measurements that have not been assigned to any of the targets, the newborn likelihood is 1 ($r_{U,k}(z) = 1$).

In the measurement-driven birth model, the newborn likelihood of $z \in Z_k$ is

$$r_{B,k+1}(z) = \min\left(r_{B_{\max}}, \lambda_{B,k+1}\cdot\frac{r_{U,k}(z)}{\sum_{\varsigma\in Z_k} r_{U,k}(\varsigma)}\right) \tag{45}$$

where $\lambda_{B,k+1}$ is the expected number of newborn targets; $r_{B_{\max}} \in [0, 1]$ is the maximum existence probability of a newborn target to ensure that $r_{B,k+1}(z)$ does not exceed 1 when $\lambda_{B,k+1}$ is too large. Generally, a larger $r_{B_{\max}}$ indicates a faster track (target) confirmation but a higher incidence of false tracks, while a smaller $r_{B_{\max}}$ indicates a slower track confirmation but a lower incidence of false tracks. The mean cardinality of the newborn GLMB is the sum of the existence probabilities

$$\sum\nolimits_{z\in Z_k} r_{B,k+1}(z) \le \lambda_{B,k+1} \tag{46}$$

New target confirmation has a time delay based on the measurement-driven model, and every clutter measurement attempts to become a new target, which makes the GLMB filter work in a harsh tracking environment.

B. PREDICTION AND UPDATE

Equation (16) provides the GLMB filtering density at time k. After the steps of new target adaptive generation and joint prediction and update, the GLMB filtering density at time $k+1$ is

$$\boldsymbol{\pi}_{Z_+}(\mathbf{X}) \propto \Delta(\mathbf{X}) \sum_{I,J,I_+,\theta_+} w^{(I,\xi)} w_{Z_+}^{(\xi,J,I_+,\theta_+)}\delta_{I_+}[\mathcal{L}(\mathbf{X})] \times\left[p_{Z_+}^{(\xi,\theta_+)}\right]^{\mathbf{X}} \tag{47}$$

where $I \in \mathcal{F}(\mathbb{L})$, $\xi \in \Xi$, $I_+ \in \mathcal{F}(\mathbb{L}_+)$, $L_+ \in \mathcal{F}(\mathbb{B})$, $\theta_+ \in \Theta_+$, and,

$$\begin{aligned} w_{Z_+}^{(I,\xi,I_+,\theta_+)} &= 1_{\Theta_+(I_+)}(\theta_+)\left[1 - \bar{P}_S^{(\xi)}\right]^{I-I_+}\left[\bar{P}_S^{(\xi)}\right]^{I\cap I_+} \\ &\quad\cdot\left[1 - r_{B,+}\right]^{\mathbb{B}_+ - I_+}\left[r_{B,+}\right]^{\mathbb{B}_+\cap I_+}\left[\bar{\varphi}_{Z_+}^{(\xi,\theta_+)}\right]^{I_+} \end{aligned} \tag{48}$$

$$\bar{P}_S^{(\xi)} = \left\langle p^{(\xi)}(\cdot, l), P_S(\cdot, l)\right\rangle \tag{49}$$

$$\bar{\varphi}_{Z_+}^{(\xi,\theta_+)}(l_+) = \left\langle \bar{p}_+^{(\xi)}(\cdot, l_+), \varphi_{Z_+}^{(\theta_+(l_+))}(\cdot, l_+)\right\rangle \tag{50}$$

$$\begin{aligned} \bar{p}_+^{(\xi)}(x_+, l_+) &= 1_{\mathbb{L}}(l_+)\frac{\left\langle P_S(\cdot, l_+) f_+(x_+|\cdot, l_+), p^{(\xi)}(\cdot, l_+)\right\rangle}{\bar{P}_S^{(\xi)}(l_+)} \\ &\quad + 1_{\mathbb{B}_+}(l_+) p_{B,+}(x_+, l_+) \end{aligned} \tag{51}$$

$$p_{Z_+}^{(\xi,\theta_+)}(x_+, l_+) = \frac{\bar{p}_+^{(\xi)}(x_+, l_+)\varphi_{Z_+}^{(\theta_+(l_+))}(x_+, l_+)}{\bar{\varphi}_{Z_+}^{(\xi,\theta_+)}(l_+)} \tag{52}$$

Equation (47) integrates all possibilities (birth, death, or survival) for each target and the one-to-one assignment between targets and measurements including missed detection.

C. MULTIPLE HYPOTHESIS TRUNCATION

At time k, we consider a fixed component (ξ, I) of the GLMB filter, $I = \{l_{1:R}\}$. At time $k+1$, the newborn target set is $\mathbb{B}_+ = \{l_{R+1:P}\}$, and the measurement set is $Z_+ = \{z_{1:M}\}$. The goal is to find a set of pairs $(I_+, \theta_+) \in \mathcal{F}(\mathbb{L}_+) \times \Theta_+(I_+)$ with significant $w_{Z_+}^{(I,\xi,I_+,\theta_+)}$.

For each pair $(I_+, \theta_+) \in \mathcal{F}(\mathbb{L}_+)\times\Theta_+(I_+)$, the association between the target and measurement can be defined by

$$\gamma_i = \begin{cases} \theta_+(l_i), & \text{if } l_i \in I_+ \\ -1, & \text{otherwise} \end{cases} \tag{53}$$

$$\psi_Z^{(j)}(x_i, l_i) = \begin{cases} \dfrac{P_D^\tau(x_i, l_i)\, g\left(z_j^{(\theta,r)}\middle| x_i, l_i\right)\left(P_D^\tau g_a^\tau\left(z_j^{(a)}\middle| d, l_i\right)\right) g_{\dot{r}}\left(z_j^{(\dot{r})}\middle| x_i, l_i\right)}{k\left(z_j^{(\theta,r)}\right)\left(P_{fa}^\tau g_a^\tau\left(z_j^{(a)}\middle| c\right)\right) g_{\dot{r}}\left(z_j^{(\dot{r})}\middle| c\right)}, & j > 0 \\ 1 - P_D^\tau(x_i, l_i), & j = 0 \end{cases} \tag{37}$$

After joint prediction and update,

$$I_+ = \{l_i \in I \cup \mathbb{B}_+ : \gamma_i > 0\}, \quad \theta_+(l_i) = \gamma_i \tag{54}$$

Assuming that for all $i \in \{1:P\}$, $\bar{P}_S^{(\xi)}(l_i) \in (0,1)$ and $\bar{P}_D^{(\xi)}(l_i)\left\langle \bar{p}_+^{(\xi)}(\cdot, l_i), P_D(\cdot, l_i)\right\rangle \in (0,1)$, the probability matrix of the one-to-one assignment between measurements (including missed detection) and targets (including new-births and deaths) can be defined as

$$\eta_i(j) = \begin{cases} 1 - \bar{P}_S^{(\xi)}(l_i), & 1 \le i \le R, j < 0 \\ \bar{P}_S^{(\xi)}(l_i)\,\bar{\psi}_{Z_+}^{(\xi,j)}(l_i), & 1 \le i \le R, j \ge 0 \\ 1 - r_{B,+}(l_i), & R+1 \le i \le P, j < 0 \\ r_{B,+}(l_i)\,\bar{\psi}_{Z_+}^{(\xi,j)}(l_i), & R+1 \le i \le P, j \ge 0 \end{cases} \tag{55}$$

where $\bar{\psi}_{Z_+}^{(\xi,j)}(l_i) = \left\langle \bar{p}_+^{(\xi)}(\cdot, l_i), \psi_{Z_+}^{(j)}(\cdot, l_i)\right\rangle; j \in \{-1:M\}$ is the index of the measurement assigned to label l_i, where $j = 0$ indicates that l_i is missed in detection, and $j = -1$ indicates that l_i no longer exists.

In the implementations of GLMB, V-GLMB, A-GLMB and MDI-GLMB, the measurement likelihood ($\psi_{Z_+}^{(j)}(\cdot, l_i)$) is given in (34), (35), (36), and (37), respectively.

According to the definition of (53) and based on (54) and (55),

$$\prod_{n=1}^{R} \eta_n(\gamma_n) = \left[1 - \bar{P}_S^{(\xi)}\right]^{I - I_+} \left[\bar{P}_S^{(\xi)} \bar{\psi}_{Z_+}^{(\xi,\theta_+)}\right]^{I \cap I_+},$$

$$\prod_{n=R+1}^{P} \eta_n(\gamma_n) = \left[1 - r_{B,+}\right]^{\mathbb{B}_+ - I_+} \left[r_{B,+} \bar{\psi}_{Z_+}^{(\xi,\theta_+)}\right]^{\mathbb{B}_+ \cap I_+}.$$

Then, (48) can be converted into

$$w_{Z_+}^{(I,\xi,I_+,\theta_+)} = 1_{\Theta_+(I_+)}(\theta_+) \prod_{i=1}^{P} \eta_i(\gamma_i) \tag{56}$$

Multiple hypothesis truncation calculates the weights ($w_{Z_+}^{(I,\xi,I_+,\theta_+)}$) of $(I_+, \theta_+) \in \mathcal{F}(\mathbb{L}_+) \times \Theta_+(I_+)$ and retains a number of hypothesis pairs with higher weights; according to (56), it can be equivalently converted into the calculation of $\prod_{i=1}^{P} \eta_i(\gamma_i)$. Furthermore, the implementation of multiple hypotheses truncation in GLMB, V-GLMB, A-GLMB and MDI-GLMB is equivalent to optimization of the association between targets and measurements.

D. FLAT GIBBS SAMPLING

Murty's method [36], [37] is often used for multiple hypothesis truncation, but it is computationally expensive and complex to implement. The Markov chain Monte Carlo (MCMC) stochastic simulation method [29], [38] is a more efficient alternative; however, in high dimensional distributions, MCMC sampling is inefficient. An efficient implementation of the GLMB filter using Gibbs sampling [26], [27] was proposed in [15]. We used Gibbs sampling to implement the MDI-GLMB filter directly, but we could not obtain good results. Now, we analyze the reasons.

TABLE 2. Flat Gibbs sampling algorithm.

Algorithm 1. Flat Gibbs

- input: $\gamma^{(1)}, N, \eta = \left[\eta_i(j)\right]$
- output: $\gamma^{(1)}, \cdots, \gamma^{(N)}$

$P := \text{size}(\eta, 1); M := \text{size}(\eta, 2); c := [-1:M]; \tilde{\eta} = \eta$
for $n = 1:N$
  $\gamma^{(n)} := []$;
  for $i = 1:P$
    for $j = 1:M$
      $\tilde{\eta}_i(j) := \eta_i(j)\left(1 - 1_{\left\{\gamma_{1:i-1}^{(n)}, \gamma_{i+1:P}^{(n-1)}\right\}}(j)\right)$;
    End
    $\tilde{\eta}_i(\tilde{\eta}_i > 1) = 1$;
    $\gamma_i^{(n)} \sim \text{Categorical}(c, \tilde{\eta}_i)$;
    $\gamma^{(n)} := \left[\gamma^{(n)}, \gamma_i^{(n)}\right]$;
  end
end

If

$$\eta_i(j_m) = \max(\eta_i) \gg 1 \tag{57}$$

where $\eta_i(j_m)$ is the likelihood probability that target i is associated with measurement j_m, then in the finite Gibbs sampling, we will likely obtain the same sample of target i associated with measurement j_m in each sampling, that is, no sample of target i has died, was missed in detection or is associated with other measurements. The finite Gibbs sampling may miss the optimal hypothesis.

In the MDI-GLMB filter, η is a generalized joint likelihood of the target position residual, signal amplitude and target radial velocity. When target i is missed, the hypothesis of $j_m = 0$ may be lost in the finite Gibbs sampling due to the coupling effect of the target position likelihood, amplitude likelihood and radial velocity likelihood (e.g., clutter with a large signal amplitude close to that of the target may lead to $\max(\eta_i) \gg 1$).

This paper proposes a flat Gibbs sampling algorithm for the MDI-GLMB filter, which can solve the drawback that finite Gibbs sampling may miss the optimal hypothesis. As the name suggests, flat Gibbs sampling aims to flatten the likelihood probability distribution η_i (e.g., $\eta_i(\eta_i > 1) = 1$) so that the optimal hypotheses can be obtained by finite sampling. where Categorical $(c, \tilde{\eta}_n)$is the likelihood probability distribution of discrete random variable c.

V. NUMERICAL STUDIES

In a circular area with a radius of 25 km, the active sonar continuously scans 100 times at regular intervals. Twelve targets (including missed detections) are simulated in a clutter

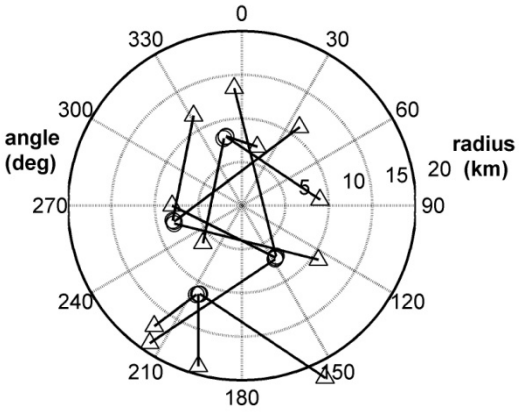

FIGURE 4. Target trajectories, where start positions for each track are shown by ○, and stop positions for each track are shown by △.

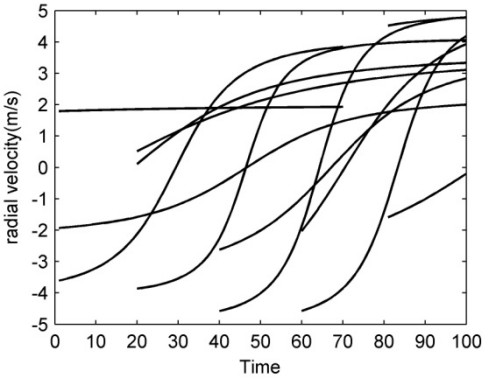

FIGURE 5. Radial velocity of each target in each probe scan.

environment to verify the effectiveness of the multidimensional information fusion algorithm. Three targets each are newly born at times $k = 1$ and $k = 20$, and two targets each are newly born at times $k = 40$, $k = 60$, and $k = 80$; among them, two targets die at time $k = 71$. Fig. 4 shows the simulated multi-object trajectories. The direction of 0° and 90° are marked as the x-axis and y-axis, respectively. Fig. 5 shows the real radial velocity of each target in each scan.

Specifically, the initial states of the 3 newborn targets at time $k = 1$ are

$$x_1^{(1)} = [-10000, -2, -5000, 0]^T,$$
$$x_1^{(2)} = [-6000, 1, 4000, -2]^T,$$
$$x_1^{(3)} = [-2000, -1, -8000, 4]^T.$$

where $x_1^{(1)}$ and $x_1^{(3)}$ die at time $k = 71$. The initial states of the 3 newborn targets at time $k = 20$ are

$$x_{20}^{(4)} = [-6000, -2, 4000, -3]^T,$$
$$x_{20}^{(5)} = [-6000, 4, 4000, -1]^T,$$
$$x_{20}^{(6)} = [-10000, -2, -5000, 3]^T.$$

The initial states of the 2 newborn targets at time $k = 40$ are

$$x_{40}^{(7)} = [-2000, 3, -8000, 4]^T,$$
$$x_{40}^{(8)} = [8000, -2, -2000, 3]^T.$$

The initial states of the 2 newborn targets at time $k = 60$ are

$$x_{60}^{(9)} = [-2000, 5, -8000, 1]^T,$$
$$x_{60}^{(10)} = [8000, -5, -2000, -1]^T.$$

The initial states of the 2 newborn targets at time $k = 80$ are

$$x_{80}^{(11)} = [-10000, -3, -5000, -4]^T,$$
$$x_{80}^{(12)} = [8000, -1, -2000, 3]^T.$$

Note that Δ represents the detection interval of the active sonar, with $\Delta = 60s$; through $x_{k+1}^{(j)} = F_k x_k^{(j)}$, we can know the real target state in each scan. Note that σ_θ, σ_r and $\sigma_{\dot{r}}$ represent the measurement error in the target azimuth, distance, and radial velocity, respectively, with $\sigma_\theta = 2 \cdot \pi/180$ (rad), $\sigma_r = 100$ (m), and $\sigma_{\dot{r}} = 0.3$ (m/s); through $z_{0k}^{(j)} = h\left(x_k^{(j)}\right) + w_k^{(j)}$, the target azimuth, distance, and radial velocity measurement can be simulated, and the target amplitude measurement $(a_k^{(j)})$ can be simulated based on the probability density function in (3). The measurement of target j at time k is $z_k^{(j)} = \left[z_{0k}^{(j)}; a_k^{(j)}\right]$; if $a_k^{(j)} < \tau$, this indicates that target j was missed at time k. Clutter is modeled as a Poisson RFS, and the locations are random with a uniform distribution. Amplitude measurement of clutter is simulated based on the probability density function in (2); the radial velocity is a Gaussian random number with zero mean and a standard-deviation of $\sigma_{\dot{r}} = 0.3$. The process noise vector of the UKF filter is $u_k = [0.005, 0.005]^T$ (m/s^2).

A. NEWBORN TARGET STATE INITIALIZATION

The initial state vector of newborn targets and their initial state covariance matrix are unknown in active sonar. Considering that a new target is driven by measurement $z = [\theta, r, \dot{r}, a]^T \in Z_k$, the state vector and state covariance matrix can be initialized as

$$m_{B,k}^{(z)} = \left[p_{x,k},\ \dot{p}_{x,k},\ p_{y,k},\ \dot{p}_{y,k}\right]^T \tag{58}$$

$$P_{B,k}^{(z)} = \begin{bmatrix} r_{xx} & 0 & r_{xy} & 0 \\ 0 & 50 & 0 & 0 \\ r_{xy} & 0 & r_{yy} & 0 \\ 0 & 0 & 0 & 50 \end{bmatrix} \tag{59}$$

where $p_{x,k} = r\cos\theta$; $\dot{p}_{x,k} = \dot{r}\cos\theta$; $p_{y,k} = r\sin\theta$; $\dot{p}_{y,k} = \dot{r}\sin\theta$; and the detailed calculations of r_{xx}, r_{xy} and r_{yy} are [39]

$$r_{xx} = \frac{1}{2}(r^2 + \sigma_r^2)(1 + \lambda'_\theta \cos 2\theta) + (\lambda_\theta^{-2} - 2)r^2\cos^2\theta,$$
$$r_{xy} = \frac{1}{2}(r^2 + \sigma_r^2)\lambda'_\theta \sin\theta + (\lambda_\theta^{-2} - 2)r^2\sin\theta\cos\theta,$$
$$r_{yy} = \frac{1}{2}(r^2 + \sigma_r^2)(1 - \lambda'_\theta \cos 2\theta) + (\lambda_\theta^{-2} - 2)r^2\sin^2\theta.$$

where $\lambda_\theta = e^{-\sigma_\theta^2/2}$; σ_θ^2 is the variance in azimuth θ; σ_r^2 is the variance in distance r; and $\lambda'_\theta = \lambda_\theta^4$.

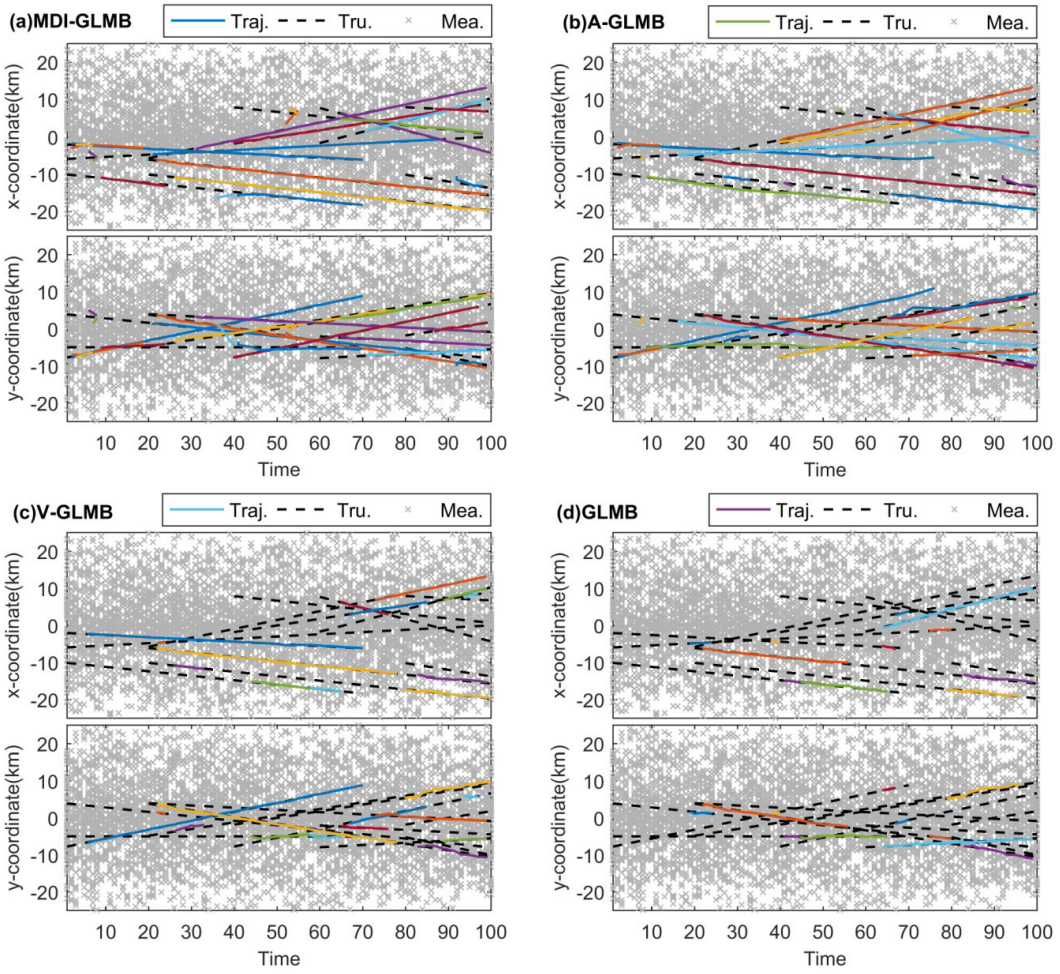

FIGURE 6. Measurements, true trajectories and tracking trajectories of the MDI-GLMB filter, A-GLMB filter, V-GLMB filter, and GLMB filter.

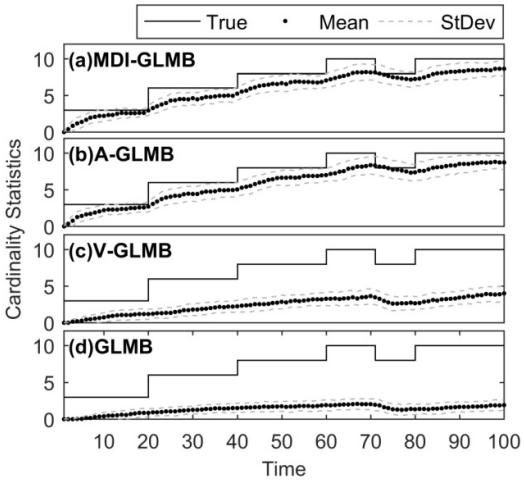

FIGURE 7. Cardinality statistics for the (a)MDI-GLMB filter, (b)A-GLMB filter, (c)V-GLMB filter, and (d)GLMB filter.

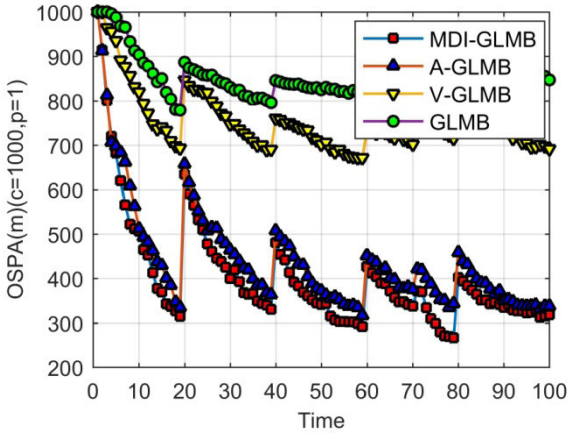

FIGURE 8. OSPA metric versus time for the MDI-GLMB filter, A-GLMB filter, V-GLMB filter, and GLMB filter.

B. WEAK TARGET SCENARIO

A numerical study of a weak target scenario is performed to verify the effectiveness of MDI-GLMB filtering for weak targets (low detection probability). In this scenario, clutter is modeled as a Poisson RFS with $\lambda_c = 3.82 \times 10^{-4} m^{-1} (rad)^{-1}$ (i.e., an average of 60 clutters per scan), probability of false alarm $P_{fa} = 0.001$, SNR of signal $1+d = 10$ (i.e., $SNR\,(\mathrm{dB}) = 10$), detection threshold $\tau = 3.7169$,

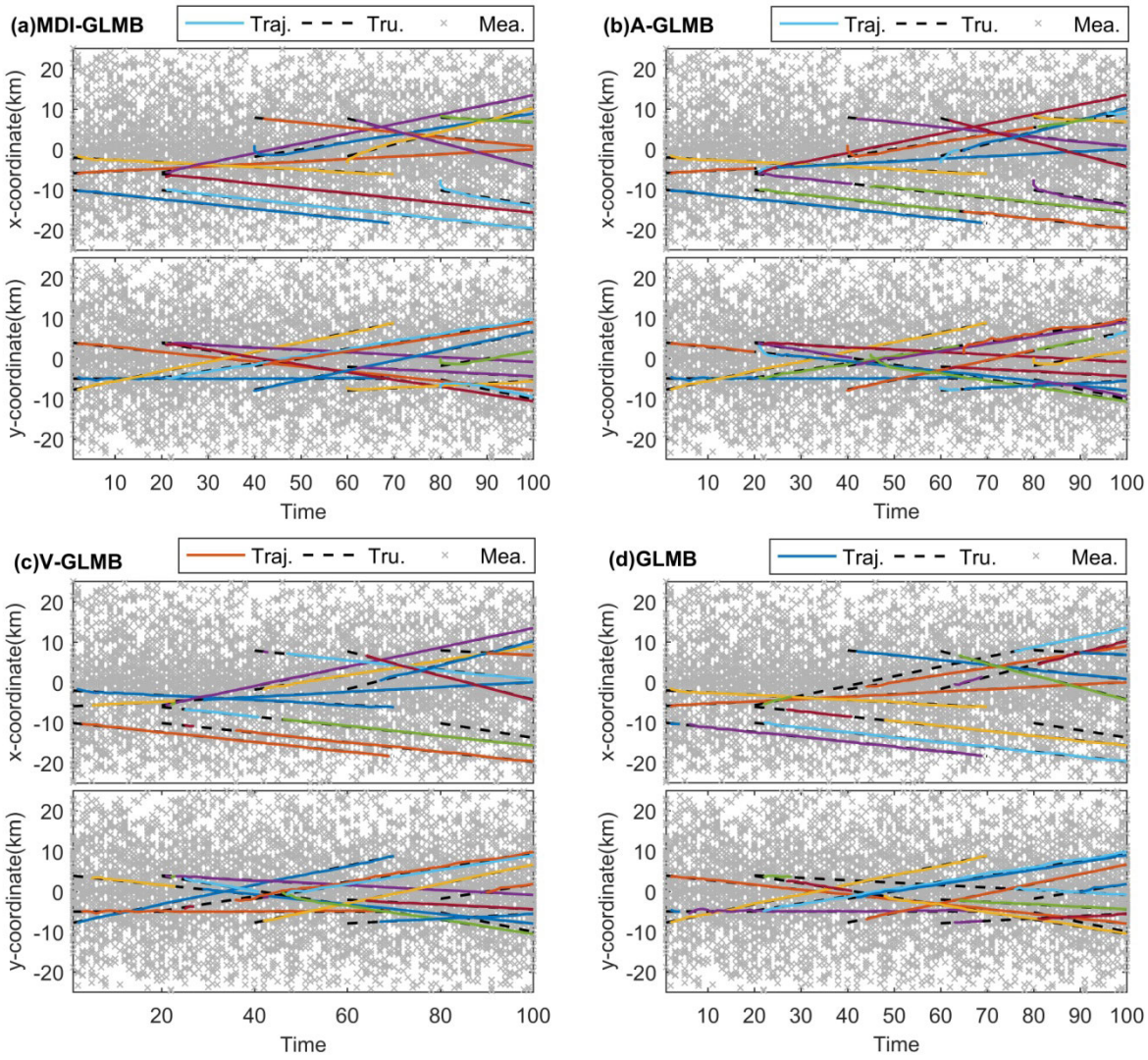

FIGURE 9. Measurements, true trajectories and tracking trajectories of the MDI-GLMB filter, A-GLMB filter, V-GLMB filter, and GLMB filter.

detection probability $P_D = 0.5337$, and survival probability $P_S = 0.95$. The expected number of newborn targets driven by measurement is $\lambda_{B,k+1} = 1$, and the maximum intensity of the newborn target is $r_{B_{\max}} = 0.1\lambda_{B,k+1}$.

Using the simulated measurement sets in the weak target scenario, we can run MDI-GLMB, A-GLMB, V-GLMB, and GLMB filtering. The tracking trajectories of each filter divided into the x component and y component versus time are shown in Fig. 6 (a)-(d). In the figure, the crosses represent measurements, the dashed lines represent the true trajectories of targets, and the straight lines represent the multi-object tracking trajectories. As the figure shows,

- After 5-20 scans of newborn target confirmation delay, the MDI-GLMB filter can estimate and track the targets with different velocities. When a target is dead, after 3-5 scans, the filter can accurately determine that the target tracking is lost. In the weak target scenario, a small number of false alarms with MDI-GLMB filtering remains.
- The filtering performance of GLMB, V-GLMB, A-GLMB, and MDI-GLMB increases in turn. In addition, the probability of target missed tracking (missed detection) of the GLMB filter is very high, which verifies the necessity and effectiveness of multidimensional information fusion for active sonar.

To verify the cardinality estimation and OSPA metric performance of the MDI-GLMB filter, we compare it with the A-GLMB, V-GLMB and GLMB filters for over 100 Monte Carlo (MC) trials. In each trial, the same target tracks in Fig. 4 are used, but a new set of measurement data is randomly generated. Fig. 7 (a)-(d) shows the mean and standard deviation of the estimated cardinality distribution versus time for the filters under study. These results confirm that the cardinality estimation performance of MDI-GLMB is slightly better than that of A-GLMB and significantly better than that of V-GLMB and GLMB. In addition, these results show that the contribution of the amplitude measurement to information

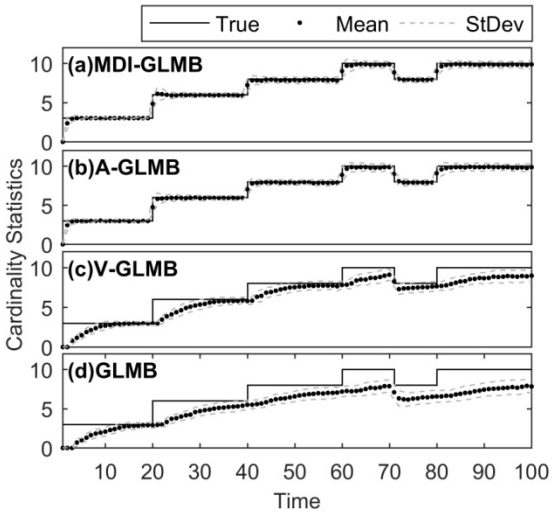

FIGURE 10. Cardinality statistics for the (a)MDI-GLMB filter, (b)A-GLMB filter, (c)V-GLMB filter, and (d)GLMB filter.

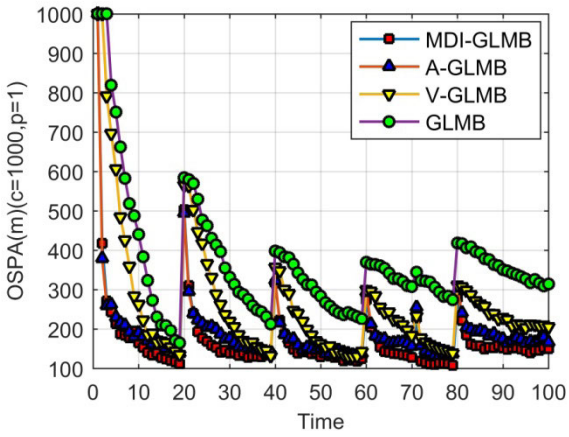

FIGURE 11. OSPA metric versus time for the MDI-GLMB filter, A-GLMB filter, V-GLMB filter, and GLMB filter.

fusion is greater than that of the radial velocity measurement, which also verifies the fusion contribution evaluation based on the KL divergence. The OSPA metrics of the four filters are compared ($p = 1, c = 1000$) in Fig. 8, which shows that MDI-GLMB has a lower OSPA metric than A-GLMB, V-GLMB and GLMB, which further verifies the effectiveness of the MDI-GLMB filter.

C. GENERAL TARGET SCENARIO

A numerical study of a general target scenario is performed to verify the effectiveness of MDI-GLMB filtering for targets with general echo strength. In this scenario, clutter is modeled as a Poisson RFS with $\lambda_c = 3.82 \times 10^{-4} m^{-1} (rad)^{-1}$, probability of false alarm $P_{fa} = 0.001$, SNR of signal $1+d = 100$ (i.e., SNR (dB) $= 20$), detection threshold $\tau = 3.7169$, detection probability $P_D = 0.9339$, and survival probability $P_S = 0.95$. The location and intensity of newborn targets are unknown. The expected number of newborn targets driven by measurement is $\lambda_{B,k+1} = 1$, and the maximum intensity of the newborn target is $r_{B_{\max}} = 0.1\lambda_{B,k+1}$.

Using the simulated measurement sets in the general target scenario, we can run MDI-GLMB, A-GLMB, V-GLMB, and GLMB filtering. The tracking trajectories of each filter divided into the x component and y component versus time are shown in Fig.9 (a)-(d). In the figure, the crosses represent measurements, the dashed lines represent real trajectories of targets, and the straight lines represent the multi-object tracking trajectories. As the figure shows,

- After 1-3 pings of newborn target confirmation delay, the MDI-GLMB filter can estimate and track the targets with different velocities. When a target is dead, after 1-3 pings, it can accurately determine that the tracking is lost. The numbers of missed detections and false alarms in MDI-GLMB filtering are very few in the general target scenario.
- MDI-GLMB has equivalent filtering performance to A-GLMB, both of which can accurately estimate the number of targets and their trajectories. The filtering performance of GLMB, V-GLMB, and A-GLMB increases in turn. In addition, the GLMB filter shows some target missed tracking, which verifies the necessity and effectiveness of the multidimensional information fusion for active sonar.

To verify the cardinality estimation and OSPA metric performance of the MDI-GLMB filter, we compare it with the A-GLMB, V-GLMB and GLMB filters for over 100 MC trials. In each trial, the same target tracks in Fig. 4 are used, but a new set of measurement data is randomly generated. Fig. 10 (a)-(d) shows the mean and standard deviation of the estimated cardinality distribution versus time for the filters under study. These results confirm that the cardinality estimation performance of MDI-GLMB is slightly better than that of A-GLMB and significantly better than that of V-GLMB and GLMB. In addition, these results show that the contribution of amplitude measurement to information fusion is greater than that of radial velocity measurement, which also verifies the fusion contribution evaluation based on the KL divergence. The OSPA metrics of the four filters are compared ($p = 1, c = 1000$) in Fig. 11, which shows that MDI-GLMB has a lower OSPA metric than A-GLMB, V-GLMB and GLMB, which further verifies the effectiveness of the MDI-GLMB filter.

VI. CONCLUSION

In this paper, a method of multidimensional information fusion in active sonar via the GLMB filter was proposed, which can accurately estimate the number of targets and their trajectories in the presence of low detection probabilities, high clutter rates, low data-sampling rates, and large measurement errors. The key innovation lies in the multidimensional measurement modeling of active sonar, which enables one to be elegantly apply the measurement information of different dimensions to the information fusion via the GLMB filter and significantly improves the filter performance. Based on the KL divergence of each dimensional measurement, we can know the necessity of fusion for a specific dimension measurement. A flat Gibbs sampling method was proposed to

efficiently implement the MDI-GLMB filter. The numerical studies show the necessity and effectiveness of the proposed MDI-GLMB filter. Future work will consider the application of the MDI-GLMB filter to real data in active sonar.

REFERENCES

[1] K. D. LePage, "Statistics of broad-band bottom reverberation predictions in shallow-water waveguides," *IEEE J. Ocean. Eng.*, vol. 29, no. 2, pp. 330–346, Apr. 2004.

[2] C. W. Holland, J. R. Preston, and D. A. Abraham, "Long-range acoustic scattering from a shallow-water mud-volcano cluster," *J. Acoust. Soc. Amer.*, vol. 122, no. 4, pp. 1946–1958, Oct. 2007.

[3] J. M. Fialkowski, R. C. Gauss, and D. M. Drumheller, "Measurements and modeling of low-frequency near-surface scattering statistics," *IEEE J. Ocean. Eng.*, vol. 29, no. 2, pp. 197–214, Apr. 2004.

[4] R. P. Hodges, *Underwater Acoustics: Analysis, Design and Performance of Sonar*. Hoboken, NJ, USA: Wiley, 2010.

[5] Y. Bar-Shalom and T. E. Fortmann, *Tracking and Data Association*. San Diego, CA, USA: Academic, 1988.

[6] S. S. Blackman and R. Popoli, *Design and Analysis of Modern Tracking Systems* (Artech House radar Library). Norwood, MA, USA: Artech House, 1999.

[7] S. S. Blackman, "Multiple hypothesis tracking for multiple target tracking," *IEEE Aerosp. Electron. Syst. Mag.*, vol. 19, no. 1, pp. 5–18, Jan. 2004.

[8] R. Mahler, *Statistical Multisource-Multitarget Information Fusion*. Norwood, MA, USA: Artech House, 2007.

[9] R. Mahler, *Advances in Statistical Multisource-Multitarget Information Fusion*. Norwood, MA, USA: Artech House, 2014.

[10] B. Ristic, M. Beard, and C. Fantacci, "An overview of particle methods for random finite set models," *Inf. Fusion*, vol. 31, pp. 110–126, Sep. 2016.

[11] R. P. S. Mahler, "Multitarget Bayes filtering via first-order multitarget moments," *IEEE Trans. Aerosp. Electron. Syst.*, vol. 39, no. 4, pp. 1152–1178, Oct. 2003.

[12] R. Mahler, "PHD filters of higher order in target number," *IEEE Trans. Aerosp. Electron. Syst.*, vol. 43, no. 4, pp. 1523–1543, Oct. 2007.

[13] B.-T. Vo, B.-N. Vo, and A. Cantoni, "The cardinality balanced multi-target multi-Bernoulli filter and its implementations," *IEEE Trans. Signal Process.*, vol. 57, no. 2, pp. 409–423, Feb. 2009.

[14] B.-N. Vo, B.-T. Vo, and D. Phung, "Labeled random finite sets and the bayes multi-target tracking filter," *IEEE Trans. Signal Process.*, vol. 62, no. 24, pp. 6554–6567, Dec. 2014.

[15] B.-N. Vo, B.-T. Vo, and H. G. Hoang, "An efficient implementation of the generalized labeled multi-Bernoulli filter," *IEEE Trans. Signal Process.*, vol. 65, no. 8, pp. 1975–1987, Apr. 2017.

[16] L. Gan and G. Wang, "Tracking the splitting and combination of group target with δ-generalized labeled multi-Bernoulli filter," *IEEE Access*, vol. 7, pp. 81156–81176, 2019.

[17] B.-T. Vo and B.-N. Vo, "Labeled random finite sets and multi-object conjugate priors," *IEEE Trans. Signal Process.*, vol. 61, no. 13, pp. 3460–3475, Jul. 2013.

[18] S. Reuter, B. T. Vo, B. N. Vo, and K. Dietmayer, "The labeled multi-Bernoulli filter," *IEEE Trans. Signal Process.*, vol. 62, no. 12, pp. 3246–3260, Dec. 2014.

[19] Z.-X. Liu and B.-J. Huang, "The labeled multi-Bernoulli filter for jump Markov systems under glint noise," *IEEE Access*, vol. 7, pp. 92322–92328, 2019.

[20] D. Schuhmacher, B.-T. Vo, and B.-N. Vo, "A consistent metric for performance evaluation of multi-object filters," *IEEE Trans. Signal Process.*, vol. 56, no. 8, pp. 3447–3457, Aug. 2008.

[21] R. Rothrock and O. E. Drummond, "Performance metrics for multiple-sensor multiple-target tracking," *Proc. SPIE*, vol. 4048, pp. 521–531, Jul. 2000.

[22] D. Clark, B. Ristic, B.-N. Vo, and B. T. Vo, "Bayesian multi-object filtering with amplitude feature likelihood for unknown object SNR," *IEEE Trans. Signal Process.*, vol. 58, no. 1, pp. 26–37, Jan. 2010.

[23] D. Clark, B. Ristic, and B.-N. Vo, "PHD filtering with target amplitude feature," in *Proc. 11th Int. Conf. Inf. Fusion*, Cologne, Germany, Jul. 2008, pp. 1–7.

[24] J. Sun, C. Liu, Q. Li, and X. Chen, "Labelled multi-Bernoulli filter with amplitude information for tracking marine weak targets," *IET Radar, Sonar Navigat.*, vol. 13, no. 6, pp. 983–991, Jun. 2019.

[25] R. Liu, H. Fan, and H. Xiao, "Labeled multi-Bernoulli filter joint detection and tracking of radar targets," *Appl. Sci.*, vol. 9, no. 19, p. 4187, Oct. 2019.

[26] T. M. Cover and J. A. Thomas, *Elements of Information Theory*. New York, NY, USA: Wiley, 1991.

[27] S. Geman and D. Geman, "Stochastic relaxation, gibbs distributions, and the Bayesian restoration of images," *IEEE Trans. Pattern Anal. Mach. Intell.*, vol. PAMI-6, no. 6, pp. 721–741, Nov. 1984.

[28] G. Casella and E. I. George, "Explaining the gibbs sampler," *Amer. Statistician*, vol. 46, no. 3, pp. 167–174, Aug. 1992.

[29] S. Oh, S. Russell, and S. Sastry, "Markov chain Monte Carlo data association for multi-target tracking," *IEEE Trans. Autom. Control*, vol. 54, no. 3, pp. 481–497, Mar. 2009.

[30] S. J. Julier and J. K. Uhlmann, "Unscented filtering and nonlinear estimation," *Proc. IEEE*, vol. 92, no. 3, pp. 401–422, Mar. 2004.

[31] M. I. Skolink, *Introduction to Radar System*, 3rd ed. New York, NY, USA: McGraw-Hill, 2002.

[32] D. Lerro and Y. Bar-Shalom, "Automated tracking with target amplitude information," in *Proc. Amer. Control Conf.*, San Diego, CA, USA, May 1990, pp. 2875–2880.

[33] B. Ristic, D. Clark, B.-N. Vo, and B.-T. Vo, "Adaptive target birth intensity for PHD and CPHD filters," *IEEE Trans. Aerosp. Electron. Syst.*, vol. 48, no. 2, pp. 1656–1668, Apr. 2012.

[34] S. Reuter, D. Meissner, B. Wilking, and K. Dietmayer, "Cardinality balanced multi-target multi-Bernoulli filtering using adaptive birth distributions," in *Proc. 16th Int. Conf. Inf. Fusion*, 2013, pp. 1608–1615.

[35] S. Lin, B. T. Vo, and S. E. Nordholm, "Measurement driven birth model for the generalized labeled multi-Bernoulli filter," in *Proc. Int. Conf. Control, Autom. Inf. Sci. (ICCAIS)*, Ansan, South Korea, Oct. 2016, pp. 94–99.

[36] K. G. Murty, "An algorithm for ranking all the assignments in order of increasing cost," *Oper. Res.*, vol. 16, no. 3, pp. 682–687, Jun. 1968.

[37] M. L. Miller, H. S. Stone, and I. J. Cox, "Optimizing Murty's ranked assignment method," *IEEE Trans. Aerosp. Electron. Syst.*, vol. 33, no. 3, pp. 851–862, Jul. 1997.

[38] B. Yang, J. Wang, and W. Wang, "An efficient approximate implementation for labeled random finite set filtering," *Signal Process.*, vol. 150, pp. 215–227, Sep. 2018.

[39] X. Sun, R. W. Li, and P. Hu, "A tracking filter method of active sonar subject to unknown target maneuver," *Acta Acoustica*, vol. 35, no. 3, pp. 265–276, 2016.

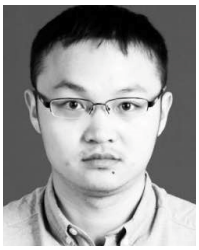

XU SUN was born in Anhui, China, in 1989. He received the bachelor's degree in mechanical engineering, in 2012, and the B.E. degree in electrical engineering, in 2015. He is currently pursuing the Ph.D. degree in electrical engineering. His research interests include multi-object tracking, multidimensional information fusion, and signal processing.

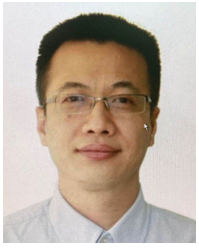

RANWEI LI was born in Heilongjiang, China, in 1967. He received the bachelor's degree in mechanical engineering, in 1990, and the B.E. degree in hydroacoustic engineering, in 1997. He is currently a Professor with the Science and Technology on Sonar Laboratory, Hangzhou Applied Acoustics Research Institute, Hangzhou, China. His research interests include signal processing, multi-object tracking, and multi-sensor data fusion.

LISHENG ZHOU was born in Neimenggu, China, in 1965. He received the bachelor's degree in theoretical physics, in 1987, and the B.E. degree in hydroacoustic engineering, in 1990. He is currently a Professor with the Science and Technology on Sonar Laboratory, Hangzhou Applied Acoustics Research Institute, Hangzhou, China. His research interests include signal processing, underwater acoustic sensor design, and multi-sensor data fusion.